ATMOSPHERIC SCIENCE

New horizons in microparticle forensics: Actinide imaging and detection of ^{238}Pu and ^{242m}Am in hot particles

Hauke Bosco[1], Linda Hamann[1], Nina Kneip[2], Manuel Raiwa[1], Martin Weiss[1], Klaus Wendt[2], Clemens Walther[1]*

Micrometer-sized pollutant particles are of highest concern in environmental and life sciences, cosmochemistry, and forensics. From their composition, detailed information on origin and potential risks to human health or environment is obtained. We combine secondary ion mass spectrometry with resonant laser ionization to selectively examine elemental and isotopic composition of individual particles at submicrometer spatial resolution. Avoiding any chemical sample preparation, isobaric interferences are suppressed by five orders of magnitude. In contrast to most mass spectrometric techniques, only negligible mass is consumed, leaving the particle intact for further studies. Identification of actinide elements and their isotopes on a Chernobyl hot particle, including ^{242m}Am at ultratrace levels, proved the performance. Beyond that, the technique is applicable to almost all elements and opens up previously unexplored scientific applications.

INTRODUCTION

Small particles in the range of few micrometers and below are released into the environment by various processes (*1*, *2*). When investigating such particles, isotope signatures of specific elements give insight into genesis, origin, and age (*3*). In the fields of radioecology and nuclear forensics, in particular, the isotope ratios of uranium, plutonium, minor actinides, and fission products are of the highest relevance. They carry information on enrichment, chemical separation, and/or interaction processes with specific neutron fields, which could take place during normal reactor operation (*4*), a nuclear explosion, or a nuclear accident (*5*, *6*). In the case of meteoritic particles, minute amounts are probed to conclude on their origin and production mechanisms from isotope ratios (*7*, *8*).

Radioactive particles pose a substantial health hazard due to inhalation when they contain alpha-emitting nuclides such as uranium, plutonium, or some minor actinides (*9*, *10*). They are mainly released by accidents in military or civil nuclear facilities. While larger fragments sediment close to the release site, particles of micrometer size and smaller might undergo long-range transport by local and global atmospheric circulation for considerable distances. For example, nuclear fuel particles from the Chernobyl accident have been detected several 1000 km away in Northern Europe (*11*).

When exposed to environmental conditions in the biosphere, depending on their chemical composition and oxidation state (*12*, *13*), some particles dissolve over time, while others remain stable over many years. Hence, detailed knowledge of their stability and analysis of the isotopic inventory of single separated particles is of great interest in various disciplines. At the same time, it is desirable that characterized particles stay intact for further analysis, e.g., for detailed chemical leaching experiments. This requires a nondestructive and ultrasensitive analysis technique as micrometer-sized particles contain only a limited number of atoms.

Scanning electron microscopy (SEM) is frequently used for localization and analyses of such micro- and nanostructures (*14*). The high spatial resolution of secondary electron detection combined with the elemental contrast of backscattered electrons (BSEs) and the analysis of characteristic x-rays by energy-dispersive x-ray spectroscopy (EDS) analysis delivers information on morphology and general elemental composition. However, EDS requires several 1000 ppm (parts per million) analyte concentration and lacks isotopic information. Nevertheless, BSE and EDS analyses allow fast localization and identification of heavy element–bearing particles. In addition, the minimal sample preparation needed for SEM and its low level of invasiveness allow for subsequent use of the unaltered analyzed material (*15*).

A great number of radioactive particles were released during the accident of 26 April 1986 in reactor block number 4 of the Chernobyl nuclear power plant (*16*–*18*). Even today, many of these so-called hot particles can be found, predominantly within the Chernobyl exclusion zone (CEZ) 30 km around the reactor (*19*, *20*). They are distinguishable from the surrounding bulk soil due to their high specific gamma activity (^{137}Cs content of the fuel particles) and due to their high density and high atomic number (fuel fragments). They are mainly composed of uranium oxide but also often contain plutonium and americium produced via neutron capture of uranium and subsequent beta decays. The alpha emitter ^{241}Am, which gives rise to an additional gamma line, continues to grow in because of the beta decay of ^{241}Pu with a half-life of 14.3 years.

A particle from the so-called Red Forest within the CEZ of ~10 μm by 10 μm by 15 μm was localized by a combination of SEM-BSE (Fig. 1) and SEM-EDS after alpha track detection. EDS proved uranium to be the main component of the particle. The alpha activity of the localized particle indicates the presence of further alpha-emitting radionuclides with half-lives much shorter than those of ^{235}U and ^{238}U, hinting at plutonium and americium isotopes. Furthermore, the BSE image revealed the structure of the particle surface. The porous structure on the nanometer scale matches that of nuclear fuel fragments rather closely. Most likely, it developed because of fission gas accumulation during the reactor operation (*21*).

[1]Institute of Radioecology and Radiation Protection, Leibniz University Hannover, Hanover, Germany. [2]Institute of Physics, Johannes Gutenberg-University Mainz, Mainz, Germany.
*Corresponding author. Email: walther@irs.uni-hannover.de

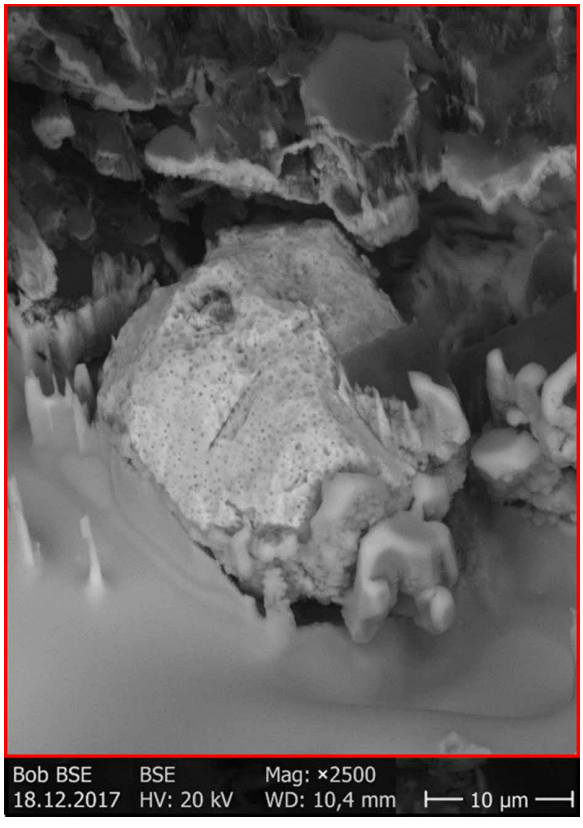

Fig. 1. SEM-BSE image of the ~10µm particle taken after localization. The bright porous structure in the center has been identified as a nuclear fuel particle. It was pressed into indium for fixation, which is visible as the smooth gray structure around it. HV, high voltage; WD, working distance.

RESULTS AND DISCUSSION

The analysis presented so far comprises of well-established routine techniques frequently reported before (*14*). In contrast to preceding work making use of subsequent destructive analysis techniques (*22*, *23*), the quasi-nondestructive static time-of-flight secondary ion mass spectrometry (TOF-SIMS) was used to determine the isotopic signature of the particle's main elemental component, uranium. The four long-lived uranium isotopes $^{234–236, 238}$U are well resolved in the mass spectrum shown in Fig. 2.

The ratios of $^{235}U/^{238}U = 0.0081(1)$ and $^{236}U/^{238}U = 0.0024(1)$ are typical for spent nuclear fuel of low initial enrichment and rather moderate burnup (*24*, *25*). The isotopes 234 to 236 do not suffer from any notable isobaric interferences apart from a minor molecular background, which is an omnipresent by-product of the sputter process (*26*). In principle, ^{238}U may interfere with ^{238}Pu. In the present case, however, this effect does not play a role for uranium isotope determination due to the high $^{238}U/^{238}Pu$ ratio, in excess of 7.5×10^4.

This advantage is reversed, when the low abundance isotopes of, e.g., plutonium and americium, are to be measured in the presence of a large excess of unwanted isobars. SIMS cannot discriminate isobars due to its nonselective ionization process. Hence, an unambiguous assignment of the peaks is not always possible as indicated in Fig. 2. For example, the species $^{238}UH^+$ might contribute, in at least a small fraction, to the peak at mass/charge ratio (m/z) = 239 assigned to ^{239}Pu. At m/z = 241, the isotopes ^{241}Pu and ^{241}Am interfere with each other. In addition, the peak at m/z = 243 is not clearly separated from the background.

Resolving these isobaric interferences is a most challenging task. Optimizing mass spectrometry for high mass resolution strongly decreases sensitivity, and chemical separation is time consuming and does not always achieve the required suppression (*27*, *28*). In the present work, multicolor laser resonant ionization (RI) was chosen for an element-selective production of ions and highly efficient suppression of isobaric interferences. Stepwise absorption of precisely tuned laser radiation selectively excites, and lastly ionizes, atoms of one specific target element for further mass separation and single ion detection (*29*–*31*).

Combining RI with SIMS is called resonant laser secondary neutral mass spectrometry (rL-SNMS), a technique also used for investigation of nuclear materials (*32*), in the field of cosmochemistry (*33*) and with low spatial resolution for plutonium imaging on clay (*34*). The sputter process produces initially formed ions and neutral atoms. The initial ions are removed by a pulsed electric field, while the neutral atoms (and molecules) form a slowly expanding cloud above the investigation spot. Pulses from three titanium:sapphire (Ti:Sa) lasers are focused into this cloud to produce "resonant ions" (*29*). The delay in the arrival of the laser pulse after the initial sputter pulse is optimized at about 0.7 µs for a balance of ionization efficiency versus suppression of unwanted diffusing secondary ions left over from the sputtering process. For further detailed technical information, see fig. S5.

Thus, rL-SNMS allows the measurement of isotope ratios of isobaric nuclides such as ^{238}Pu and ^{238}U at trace concentrations, something not possible by conventional low-resolution mass spectrometry. By alternately tuning the laser excitation to the resonances of different elements, which recently became possible within a few minutes for access to most of the elements by a thoughtful selection of the excitation schemes, power density, and relative laser beam polarizations (*35*), an effective suppression of isobaric interferences of typically more than five orders of magnitude is achieved. The ionization efficiency in SNMS may vary slightly for different isotopes of an element (*36*, *37*) and can be compensated by calibration measurements if needed.

In the following section, the use of rL-SNMS to measure the plutonium isotope composition of the Chernobyl particle is presented. The lasers were tuned to plutonium resonances, yielding a spectrum of plutonium isotopes at a mass resolution well above 1000 (see Fig. 3). The spectrum in red was acquired with all lasers tuned to the corresponding resonant transitions of plutonium for efficient RI. The nonresonant background (black) was measured by detuning the first-step laser, which normally drives the excitation from the ground state to the first excited state (FES), off resonance by 150 GHz (table S1), while all other parameters were kept constant. The main isotopes, $^{239-242}$Pu, were detected almost background free. The unexpected peak at m/z = 238.5 in both spectra originates from a small leftover fraction of the vast surplus of $^{238}U^+$ secondary ions, which was not fully suppressed but left over from the initial sputter process. The slight adjustments in the electric fields for ion extraction during SNMS versus SIMS shift this peak to the apparent m/z = 238.5. The m/z = 238 SNMS signal is clearly composed of two contributions: first, the resonantly ionized ^{238}Pu, and second, the nonresonantly ionized ^{238}U atoms. By simple background subtraction, the fraction of ^{238}Pu is calculated.

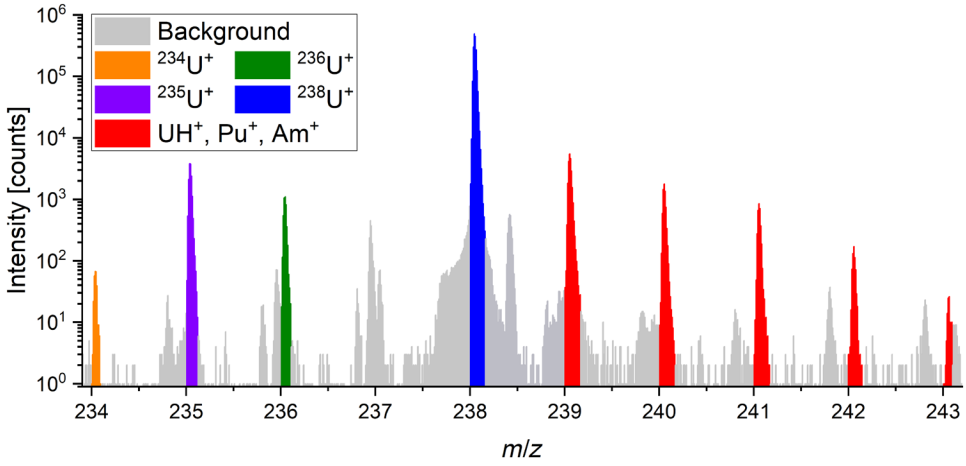

Fig. 2. TOF-SIMS spectrum of the hot particle. The spectrum represents a region-of-interest analysis of the particle's uranium signal. The uranium peak areas are marked in individual colors for the different isotopes. In addition, the masses of higher actinides with isobaric interferences are marked in red.

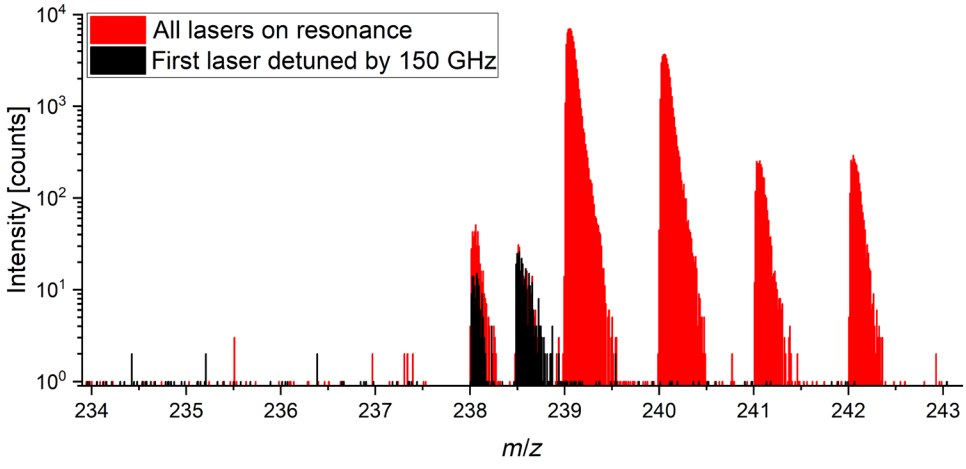

Fig. 3. Resonant laser–SNMS with the lasers tuned to plutonium resonances. The spectrum in red was acquired with all lasers stabilized on the corresponding resonances. The spectrum in black was acquired under the same conditions as the resonant signal with one exception. The laser for the first excitation step was detuned by 150 GHz off the resonance frequency.

In comparison to the conventional SIMS spectrum given in Fig. 2, the relative ion signal strength at m/z = 241 is substantially reduced in the rL-SNMS spectrum compared to the neighboring mass peaks. This is not an artifact but rather additional proof of the high element selectivity of rL-SNMS. Conventional SIMS does not discriminate between isobars. Hence, ^{241}Pu (half-life 14.3 years) and its decay product ^{241}Am both contribute to the peak at m/z = 241 (Fig. 2). rL-SNMS tuned to Pu resonances, however, fully suppresses the americium fraction. This explanation is further corroborated by the absence of any peak at m/z = 243 despite the known presence of ^{243}Am in the particle (see below).

The plutonium isotope ratios calculated from the peak areas in Fig. 3 are given in Table 1. Previously, synthetic samples with a U/Pu ratio of only 10 were analyzed (*38*). The present measurement reports a direct mass-spectrometric determination of ^{238}Pu in an environmental sample without the need for elaborate chemical pretreatment and at a much more challenging U/Pu ratio than in (*38*).

By comparing the results to the ones obtained from the destructive analysis of macroscopic amounts of reaktor bolshoy moshchnosti kanalnyy "high-power channel-type reactor" (RBMK) fuel (*39*), the suppression ratio for uranium has been estimated. The particle's plutonium isotope ratios are very close to the ones of sample 9 of the analyzed RBMK fuel samples in Makarova *et al.* (*39*), which are included in Table 1. For comparison with these reference values, decay corrections were performed. The content of ^{238}U per ton of initial uranium (U_0) was determined to be 974.7(15) kg/t_{U0}, whereas the ^{238}Pu content was given as only 12.8(2) g/t_{U0}. Assuming the nonresonant laser-dependent background of 194 counts at m/z = 238 to be solely caused by the enormous ^{238}U surplus and ascribing the resonant excess of 202 counts to ^{238}Pu, the suppression of the isobaric interference ^{238}U against ^{238}Pu is estimated to be about 75,000. Almost five orders of magnitude in isobaric suppression are obtained without any chemical separation and with the particle remaining quasi-intact.

Americium

All rL-SNMS measurements on plutonium presented above were performed in the so-called spectrometry mode of the primary ion beam, limited to a spatial resolution of about 5 μm, with a mass

Table 1. Isotope inventory of plutonium. Integrated signal counts in the peak areas of the spectrum of Fig. 3 as measured, together with nonresonant background. Extracted ratios are compared to expected values from Makarova *et al.*, sample 9 from table 7 including decay correction (*39*).

	^{238}Pu	^{239}Pu	^{240}Pu	^{241}Pu	^{242}Pu
Signal [measured counts]	396	68,084	36,148	2387	2636
Background [measured counts]	194	11	1	1	1
Rel. content [%] this work	0.22(3)*	57.2(2)	30.4(2)	10.0(2)*	2.21(4)
Rel. content [%] from (*39*)	0.288(6)	59.23(11)	30.12(6)	8.13(16)	2.23(5)
Mass [g/t_{HWM}] from (*39*)	12.8(2)	2290(30)	1165(12)	315(5)	86.1(2)

*Values were decay-corrected back to 26 April 1986.

resolution of ca. 4000. In this way, isotopic contents can be determined with low statistical uncertainty. Alternatively, in the so-called fast imaging mode (*40*), the primary ion beam spot can be focused down to ca. 100 nm on the target for spatial resolution of specific details in the isotopic or molecular sample composition. By two-dimensional imaging of the ion intensity of a given mass interval, the structure of the analyzed sample and the spatial origin of the individual isotopes can be imaged. The trace isotope ^{241}Am was screened by rL-SNMS in fast imaging mode while, simultaneously, the nonresonantly laser ionized uranium oxide signal was recorded. A further minor experimental modification concerned the choice of laser excitation: Two externally frequency doubled Ti:Sa lasers emitting radiation in the blue spectral range were used to excite a two-step RI scheme (*41*) instead of three steps. A clear spatial correlation of $^{238}UO^+$ and $^{241}Am^+$ was observed. The ion images given in Fig. 4 show very similar patterns. This leads to the conclusion that the vast majority of ions detected originate from the particle itself and that no substantial contamination from any object located close by was measured. Furthermore, some fine details in the surface structure are revealed, which match the ones observed by SEM (such as depicted in Fig. 1). Note that for exact comparison of the images of SEM and SNMS, the 45° angle of view by SNMS and some minor distortions originating from the effective acceleration field geometry need to be considered.

Following the ion imaging, additional mass spectra were recorded in spectrometry mode (Fig. 5). Apart from the two-step excitation, the experimental setup for rL-SNMS on americium and curium isotopes was identical to the conditions for plutonium analysis. As mentioned before, the particle's high specific alpha activity already suggests the presence of alpha-emitters with half-lives considerably shorter than the ones of ^{238}U or ^{235}U, which is confirmed by the observation of ^{241}Am and ^{243}Am (Fig. 5, top, red mass spectrum). Only minor nonresonant background shows up on the plutonium masses m/z = 239 to 242 (black).

In comparison to the plutonium spectrum of Fig. 3, the americium peaks show a slightly enhanced tailing caused by a setting optimized for signal-to-background ratio. Nevertheless, the isotopes are clearly separated.

In addition to the expected peaks of americium at m/z = 241 and 243, the resonant spectrum shows an unexpected resonant enhancement of the ion signal at m/z = 242 by 348 excess counts (red minus black spectrum). A selective RI of molecules with this m/z can be excluded, because only atoms are selectively resonantly ionized by rL-SNMS. Any explanation based solely on non-RI of ^{242}Pu can also be ruled out: The plutonium peaks at m/z = 239 and 240 do not change for the red (resonantly tuned to americium) versus the black (nonresonant) spectra; hence, there is no reason to expect the ^{242}Pu contribution to change. Non-RI of ^{226}RaO is ruled out for two reasons: Only ca. 10^{-6} g/t are expected in spent fuel [data for boiling water reactor (BWR) spent fuel in (*42*)] and a nonresonant production would not change upon detuning of the first laser. Consequently, there has to be an americium isotope causing the excess in the m/z = 242 peak in the red spectrum. The only americium isomer at mass 242 still detectable 34 years after the accident is ^{242m}Am with a half-life of 141 years (*43*). This isotope has a production path with rather low probability as shown in Fig. 6. It originates from a minor neutron capture branch (10%) of ^{241}Am, which, in turn, is the beta-decay product of ^{241}Pu produced during reactor operation (*44*, *45*). The total abundance of ^{242m}Am lies in the range of a few mg/t_{U0}, depending on burnup. The low beta-decay energies together with the low abundance make ^{242m}Am extremely difficult to detect radiometrically (*46*, *47*). In the present work, ^{242m}Am has been detected in a fuel sample without any chemical pretreatment. The isotopic signature of americium measured in this work is given in Table 2. As no ^{242m}Am data were given by Makarova *et al.* (*39*), the reference value for ^{242m}Am was calculated based on the ^{242}Cm and ^{243}Am data [4.7 g/t_{U0} of ^{243}Am according to (*39*)] and following a suggestion by Bowen *et al.* (*48*). Assuming a particle volume of 1.5×10^{-9} cm^3 and a density similar to UO_2 with 11 g/cm^3, the total estimated mass of the particle amounts to 16.5 ng. Combined with the calculated ^{242m}Am mass fraction of 0.18 g/t_{U0} according to Makarova *et al.* (*39*), the total content of ^{242m}Am in the particle is thus estimated to be only 3 fg (ca. 10^7 atoms) and ca. 80 fg ^{243}Am.

Stimulated by a specific two-step resonant excitation scheme for curium developed at the Institute of Physics, Johannes Gutenberg University Mainz, a measurement of the ultralow level isotope ^{244}Cm was performed to quantify the production mechanisms described in Fig. 6. The transition energies and laser powers are given in table S1. The mass spectrum in Fig. 5 (bottom) shows that on resonance, a total of 41 counts were detected on m/z = 244 at a background of just 10 counts in the nonresonant measurement, which points to a successful identification of ^{244}Cm in the sample. Using the particle mass of 16.5 ng estimated above and the measured mass fraction of 0.6 g/t_{U0} of ^{244}Cm in RBMK-fuel, as given by Makarova *et al.* (*39*) in sample 9, the total mass of ^{244}Cm corresponds to 2.7 fg present in the particle at the time of measurement (decay-corrected).

For the americium as well as for the curium measurement by rL-SNMS, only a very small amount of sample from the particle's surface is consumed. This is demonstrated by comparing SEM

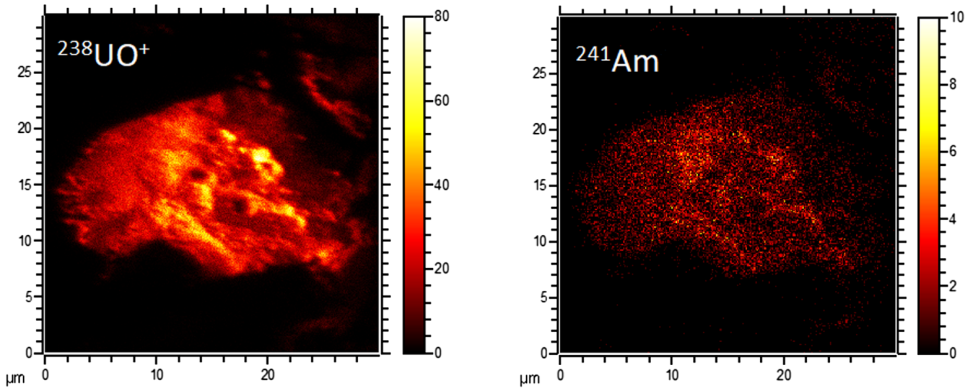

Fig. 4. Ion images of uranium oxide and ^{241}Am. Images were created from a fast-imaging measurement in combination with resonance ionization of americium. The left-hand image shows the spatial distribution of the nonresonantly ionized UO^+ signal, and the right-hand image shows the resonantly ionized $^{241}Am^+$ signal.

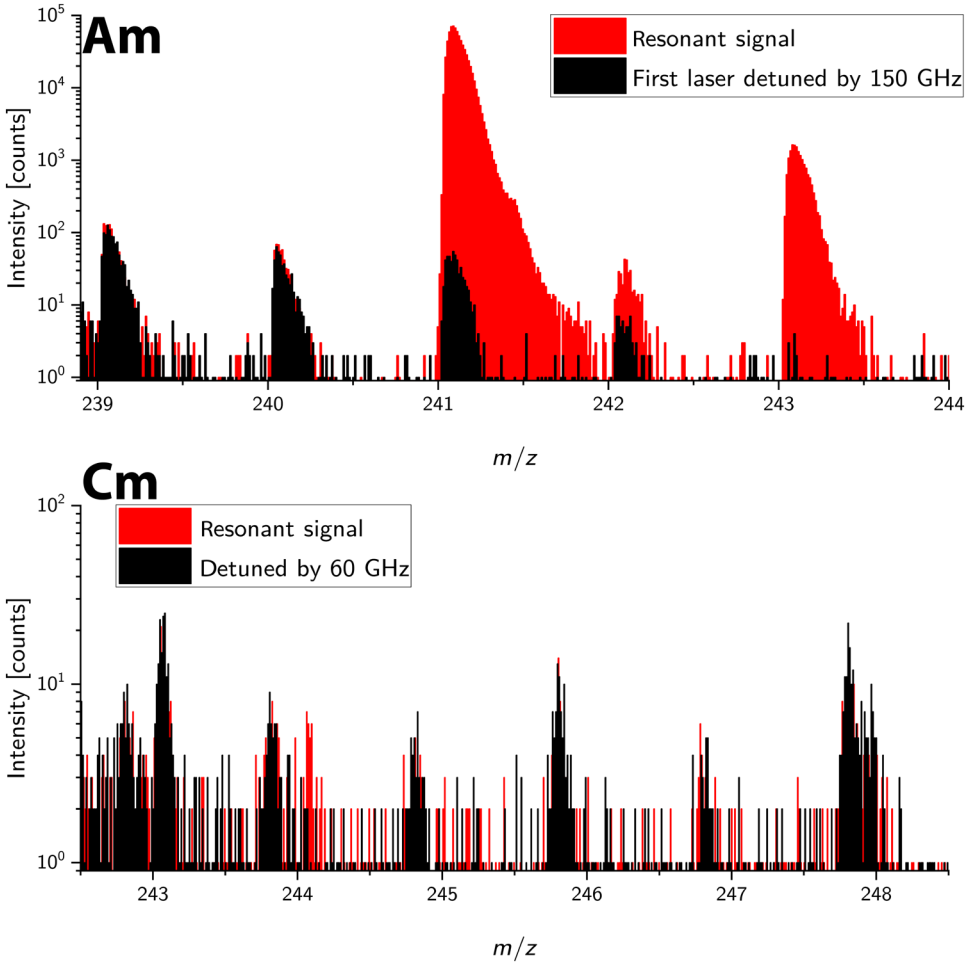

Fig. 5. Resonant laser–SNMS with the lasers tuned to americium (top) and curium (bottom) resonances. The mass spectra are overlays of resonant and a nonresonant SNMS spectrum in analogy to the plutonium case in Fig. 3. The particle contained ca. 80 fg ^{243}Am, 3 fg ^{242m}Am, and ca. 2.7 fg curium. The high background in the bottom spectrum is due to increased laser power needed for curium detection.

images of a second and much smaller particle in fig. S3 before and after obtaining plutonium and americium spectra (the latter is depicted in fig. S4). In the case of curium analysis, this means that orders of magnitude less than the estimated 2.7-fg curium content of the whole particle are consumed to obtain the rL-SNMS spectrum.

The detection and localization of ultratrace concentrations of radioactive actinides on the 100-nm scale have been demonstrated on a hot particle with minimal sample consumption. SEM analysis as well as TOF-SIMS and rL-SNMS analysis were combined, keeping the original particle sample intact for further analyses. Miniscule

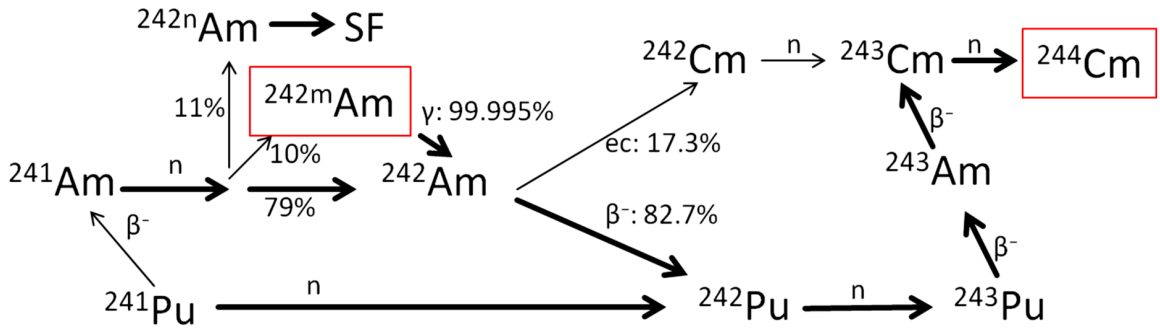

Fig. 6. Production scheme of ^{242m}Am and ^{244}Cm. Neutron capture induced nuclear reactions of ^{241}Am from ^{242m}Am. ^{244}Cm forms via beta decay of ^{243}Pu followed by subsequent neutron capture. SF stands for spontaneous fission. Only decay channels relevant for production of ^{242m}Am and ^{244}Cm are shown. Transition probabilities are taken from calculations and measurements (*49*). ec, electron capture.

Table 2. Isotope content of the particle in the americium region. Peak areas taken from the mass spectrum of Fig. 5.

	Mass 239	Mass 240	^{241}Am	^{242m}Am	^{243}Am
Signal [counts]	1177	555	724,475	348	16,435
Background [counts]	1097	484	561	66	23
Rel. content [%] this work	-	-	97.73(1)	0.04(1)	2.24(1)
Rel. content [%] from (*39*)	-	-	97.702(1)*	0.049(1)†	2.249(1)
Mass [g/t $_{U0}$] from (*39*)	-	-	251.8(40)*	0.18(1)†	4.7(1)‡

*Values calculated from ^{241}Pu masses taken from table 7 of Makarova *et al.* (*39*). †Values calculated from ^{242}Cm values of Makarova *et al.* (*39*). ‡Values taken from table 8 of Makarova *et al.* (*39*).

amounts of isotopes contained within the particle were unambiguously identified, and distributions within the hot particle were imaged in ion maps. Without any sample preparation, minor trace isotopes like ^{238}Pu, ^{242m}Am, or ^{244}Cm were detected with lowest isobaric interferences. In the assessment of these findings, one has to keep in mind that the information is obtained from the particle's surface and may not necessarily be representative for the entire particle. On the other hand, influences resulting from leaching processes or precipitation at the sample surface could be measured by depth profiling. The isotopic signatures given here allow further interpretation: Americium forming during reactor operation (^{243}Am) is built and fixed into the uranium oxide lattice. ^{241}Am formed after the accident via decay of ^{241}Pu might be easier to leach from the particle. However, because the ^{241}Am/^{243}Am isotope ratios (Table 2) still agree with the (decay-corrected) bulk data obtained in (*39*), no isotope selective losses during the 30-year weathering period occurred.

For future investigations of isotopic chemical stability from a single particle, sequential chemical extraction, or leaching, will be performed. This becomes possible by the fact that only a thin surface layer is consumed by SNMS firmly preserving the particle for subsequent investigations.

This work took several iterations of refinement of measurement conditions to reach the actual rather optimum state with now a minimum of time consumption in sample handling and data acquisition. A sample can be prepared via particle extraction and separation from the surrounding matrix within 1 to 2 hours. Subsequent transfer into the TOF-SIMS for determination of isotopic signatures additionally takes 1 to 2 hours for general analysis by TOF-SIMS and 4 hours of plutonium, americium, and curium analysis by rL-SNMS, with a tuning time of only a few minutes between elements due to the use of grating Ti:Sa lasers. Hence, under optimum conditions, a full sample analysis including preparation of a single particle sample, SEM imaging, EDS analysis, TOF-SIMS, and rL-SNMS for few elements, e.g., plutonium, americium, curium, or, for example, lanthanides or other fission products, is achievable within one working day. This makes this new technique attractive not only as a routine tool for nuclear forensics but also as part of emergency preparedness.

MATERIALS AND METHODS

Sampling was performed in the CEZ (N51°22′59″, E30°4′42″). Soil samples were gradually sieved, and the smallest fraction exhibiting the highest specific activity was separated and pressed into indium foil for fixation (Haines & Maassen, In 99.99%, 100 μm thickness). After localization by alpha track detection using CN-85 cellulose nitrate detectors by Kodak, the particles were extracted with a biopsy punch. The sample was fixed on an aluminum block and exposed to a new alpha track detector for another 15 min (fig. S1). Exposed detectors were etched in 10% sodium hydroxide solution at 60°C for 22 min and rinsed subsequently with high-purity water for another 22 min. The alpha tracks in the detector material were analyzed by a light microscope LV DAF (Nikon) (fig. S1). The sample was transferred to an environmental scanning electron microscope ESEM XL-30 (Philips). BSE images were recorded in high vacuum mode at 10^{-3} mbar (Fig. 1 and fig. S2).

TOF SIMS and rL-SNMS

All analyses were performed in a TOF.SIMS5 (IONTOF). The mass spectrometer is equipped with a Bi Nanoprobe liquid metal ion gun (Bi_3^+ ion pulses at 30 kV impinging onto the surface at a 45° angle of incidence). The mass spectrometer can be operated at spectrometry mode (high mass resolution, high ion transmission, and low lateral resolution of a few micrometers) or in fast imaging mode (high lateral resolution, low primary, and secondary ion fluxes). The mass spectra given in Figs. 2, 3, and 5 were obtained in spectrometry mode at a pixel count of 128 × 128 and a measurement window of 30 μm by 30 μm.

rL-SNMS

Three Ti:Sa lasers individually pumped by DM60-532 internally frequency doubled Nd:YAG lasers (photonics industries) are tuned to wavelengths according to table S1, evaluated by a WS6-600 (HighFinesse) wavemeter. The temporal overlap of the Ti:Sa laser pulses was realized by synchronizing the trigger signal of the pump lasers relative to a master trigger signal of the SIMS with a delay generator DG645 [Stanford Research Systems (SRS)]. For each mass spectrum, two measurements were taken and combined in an overlay. The first measurement was taken with all lasers stabilized on their corresponding resonance frequency. A second measurement of identical duration was taken directly afterward with the laser exciting the transition from the ground state to the FES slightly detuned (table S1).

Imaging

The exact calibration of the lateral resolution in rL-SNMS images cannot be realized because of a lack of an americium or plutonium lateral resolution calibration standard. In SIMS mode, a dedicated copper mesh structure is used for adjustment and calibration purposes. After the adjustment and calibration of the ion source, the timing of the ion pulse is changed relative to the suppression and following extraction field. Hence, the effective field changes and causes a lateral distortion in the *x* direction, distorting (stretching) the resulting ion image in the *x* direction. Therefore, the rL-SNMS ion images are slightly magnified relative to SIMS and SEM images.

SUPPLEMENTARY MATERIALS

Supplementary material for this article is available at https://science.org/doi/10.1126/sciadv.abj1175

REFERENCES AND NOTES

1. P. H. M. Hoet, I. Brüske-Hohlfeld, O. V. Salata, Nanoparticles—Known and unknown health risks. *J. Nanobiotechnol.* **2**, 12 (2004).
2. H. Geckeis, T. Rabung, T. Schäfer, Actinide-nanoparticle interaction: Generation, stability and mobility, in *Actinide Nanoparticle Research*, S. Kalmykov, M. Denecke, Eds. (Springer, 2011), pp. 1–30.
3. D. Lal, The oceanic microcosm of particles. *Science* **198**, 997–1009 (1977).
4. K. Mayer, M. Wallenius, K. Lützenkirchen, J. Horta, A. Nicholl, G. Rasmussen, P. van Belle, Z. Varga, R. Buda, N. Erdmann, J.-V. Kratz, N. Trautmann, L. K. Fifield, S. G. Tims, M. B. Fröhlich, P. Steier, Uranium from german nuclear power projects of the 1940s—A nuclear forensic investigation. *Angew. Chem. Int. Ed. Eng.* **54**, 13452–13456 (2015).
5. A. Axelsson, D. Fischer, M. Peńkin, Use of data from environmental sampling for IAEA safeguards. Case study: Uranium with near-natural 235U abundance. *J. Radioanal. Nucl. Chem.* **282**, 725–729 (2009).
6. M. Wallenius, K. Mayer, Origin determination of plutonium material in nuclear forensics. *J. Radioanal. Nucl. Chem.* **246**, 317–321 (2000).
7. N. Liu, T. Stephan, S. Cristallo, R. Gallino, P. Boehnke, L. R. Nittler, C. M. O. Alexander, A. M. Davis, R. Trappitsch, M. J. Pellin, I. Dillmann, Presolar silicon carbide grains of types Y and Z: Their molybdenum isotopic compositions and stellar origins. *Astrophys. J.* **881**, 1–14 (2019).
8. L. Qin, L. R. Nittler, C. M. O. Alexander, J. Wang, F. J. Stadermann, R. W. Carlson, Extreme 54Cr-rich nano-oxides in the CI chondrite Orgueil—Implication for a late supernova injection into the solar system. *Geochim. Cosmochim.* **75**, 629–644 (2011).
9. W. Burkart, H. Linder, Hot particles in the environment: Assessment of dose and health detriment. *Soz. Praventivmed.* **32**, 310–315 (1987).
10. M. W. Charles, A. J. Mill, P. J. Darley, Carcinogenic risk of hot-particle exposures. *J. Radiol. Prot.* **23**, 5–28 (2003).
11. H. Saari, S. Luokkanen, M. Kulmala, S. Lehtinen, T. Raunemaa, Isolation and characterization of hot particles from Chernobyl fallout in Southwestern Finland. *Health Phys.* **57**, 975–984 (1989).
12. A. Kersting, Plutonium transport in the environment. *Inorg. Chem.* **52**, 3533–3546 (2013).
13. B. Salbu, O. C. Lind, Radioactive particles released into the environment from nuclear events, in *Actinide Nanoparticle Research*, S. Kalmykov, M. Denecke, Eds. (Springer, 2011), pp. 335–359.
14. International Atomic Energy Agency, (IAEA), "Radioactive particles in the environment: Sources, particle characterization and analytical techniques" (IAEA-TECDOC-1663, IAEA, 2011).
15. V. Zheltonozhsky, K. Mück, M. Bondarkov, Classification of hot particles from the Chernobyl accident and nuclear weapons detonations by non-destructive methods. *J. Environ. Radioact.* **57**, 151–166 (2001).
16. F. J. Sandalls, M. G. Segal, N. Victorova, Hot particles from Chernobyl: A review. *J. Environ. Radioact.* **18**, 5–22 (1993).
17. V. A. Kashparov, Y. A. Ivanov, S. I. Zvarisch, V. P. Protsak, Y. V. Khomutinin, A. D. Kurepin, E. M. Pazukhin, Formation of hot particles during the Chernobyl nuclear power plant accident. *Nucl. Technol.* **114**, 246–253 (1996).
18. P. Carbol, D. Solatie, N. Erdmann, T. Nylén, M. Betti, Deposition and distribution of Chernobyl fallout fission products and actinides in a Russian soil profile. *J. Environ. Radioact.* **68**, 27–46 (2003).
19. A. Bulgakov, A. Konoplev, J. Smith, G. Laptev, O. Voitsekhovitch, Fuel particles in the Chernobyl cooling pond: Current state and prediction for remediation options. *J. Environ. Radioact.* **100**, 329–332 (2009).
20. J. A. Entwistle, A. G. Flower, G. Nageldinger, J. C. Greenwood, Identification and characterization of radioactive 'hot' particles in Chernobyl fallout contaminated soils: The application of two novel approaches. *Mineral. Mag.* **67**, 183–204 (2003).
21. J. Rest, M. W. D. Cooper, J. Spino, J. A. Turnbull, P. Van Uffelen, C. T. Walker, Fission gas release from UO2 nuclear fuel: A review. *J. Nucl. Mater.* **513**, 310–345 (2019).
22. F. Esaka, K. T. Esaka, C. G. Lee, M. Magara, S. Sakurai, S. Usuda, K. Watanabe, Particle isolation for analysis of uranium minor isotopes in individual particles by secondary ion mass spectrometry. *Talanta* **71**, 1011–1015 (2007).
23. S. Konegger-Kappel, T. Prohaska, Spatially resolved analysis of plutonium isotopic signatures in environmental particle samples by laser ablation-MC-ICP-MS. *Anal. Bioanal. Chem.* **408**, 431–440 (2016).
24. V. Mironov, S. Pribylev, V. Zhuravkov, J. Matusevich, M. Hotchkis, D. Child, The use of ^{236}U as a tracer of irradiated uranium, in *Radioactive Particles in the Environment*, D. H. Oughton, V. Kashparov, Eds. (Springer, 2009).
25. S. F. Boulyga, J. S. Becker, Determination of uranium isotopic composition and 236U content of soil samples and hot particles using inductively coupled plasma mass spectrometry. *Fresenius J. Anal. Chem.* **370**, 612–617 (2001).
26. D. A. Reed, J. E. Baker, Use of ISS and doubly charged secondary ions to monitor surface composition during SIMS analyses. *Nucl. Inst. Methods Phys. Res. A* **218**, 324–326 (1983).
27. T. Ohno, M. Hirono, S. Kakuta, S. Sakata, Determination of strontium 90 in environmental samples by triple quadrupole ICP-MS and its application to Fukushima soil samples. *J. Anal. At. Spectrom.* **33**, 1081–1085 (2018).
28. C. Walther, K. Wendt, Radioisotope Mass Spectrometry in *Handbook of Radioactivity Analysis*, M. F. L'Annunziata, Ed. (Academic Press, ed. 4, 2020), vol. 1, chap. 8.
29. M. Franzmann, H. Bosco, C. Walther, K. Wendt, A new resonant laser-SNMS system for environmental ultra-trace analysis: Installation and optimization. *Int. J. Mass Spectrom.* **423**, 27–32 (2017).
30. S. Raeder, A. Hakimi, N. Stöbener, N. Trautmann, K. Wendt, Detection of plutonium isotopes at lowest quantities using in-source resonance ionization mass spectrometry. *Anal. Bioanal. Chem.* **404**, 2163–2172 (2012).
31. K. Wendt, T. Gottwald, C. Mattolat, S. Raeder, Ionization potentials of the lanthanides and actinides—Towards atomic spectroscopy of super-heavy elements. *Hyperfine Interact.* **227**, 55–67 (2014).
32. M. R. Savina, B. H. Isselhardt, A. Kucher, R. Trappitsch, B. V. King, D. Ruddle, R. Gopa, I. Hutcheon, High useful yield and isotopic analysis of uranium by resonance ionization mass spectrometry. *Anal. Chem.* **89**, 6225–6232 (2017).
33. T. Stephan, R. Trappitsch, A. M. Davis, M. J. Pellin, D. Rost, M. R. Savina, R. Yokochi, N. Liu, CHILI—The Chicago Instrument for Laser Ionization—A new tool for isotope measurements in cosmochemistry. *Int. J. Mass Spectrom.* **407**, 1–15 (2016).
34. D. Schönenbach, F. Berg, M. Breckheimer, D. Hagenlocher, P. Schonberg, R. Haas, S. Amayri, T. Reich, Development, characterization, and first application of a resonant laser secondary neutral mass spectrometry setup for the research of plutonium in the context of long-term nuclear waste storage. *Anal. Bioanal. Chem.* **413**, 3987–3997 (2021).

35. H. Bosco, M. Weiss, M. Raiwa, C. Walther, N. Kneip, K. Wendt, Influence of the hyperfine structure on plutonium in resonant laser-SNMS. *Hyperfine Interact.* **241**, 34 (2020).
36. A. Lyras, B. Zorman, P. Lambropoulos, Theory of doubly resonant ionization by broad-band radiation applied to the determination of isotopic abundances. *Phys. Rev. A* **42**, 543–549 (1990).
37. R. K. Wunderlich, I. D. Hutcheon, G. J. Wasserburg, G. A. Blake, Laser-induced isotopic selectivity in the resonance ionization of Os. *Int. J. Mass Spectrom. Ion Process.* **115**, 123–155 (1992).
38. B. H. Isselhardt, M. R. Savina, A. Kucher, S. D. Gates, K. B. Knight, I. D. Hutcheon, Improved precision and accuracy in quantifying plutonium isotope ratios by RIMS. *J. Radioanal. Nucl. Chem.* **307**, 2487–2494 (2016).
39. T. P. Makarova, B. A. Bibichev, V. D. Domkin, Destructive analysis of the nuclide composition of spent fuel of WWER-440, WWER-1000, and RBMK-1000 reactors. *Radiochemistry* **50**, 414–426 (2008).
40. F. Kollmer, W. Paul, M. Krehl, E. Niehuis, Ultra high spatial resolution SIMS with cluster ions—Approaching the physical limits. *Surf. Interface Anal.* **45**, 312–314 (2012).
41. N. Kneip, C. E. Düllmann, V. Gadelshin, R. Heinke, C. Mokry, S. Raeder, J. Runke, D. Studer, N. Trautmann, F. Weber, K. Wendt, Highly selective two-step laser ionization schemes for the analysis of actinide mixtures. *Hyperfine Interact.* **241**, 45 (2020).
42. F. Peiffer, B. McStocker, D. Gründler, F. Ewig, B. Thomauske, A. Havenith, J. Kettler, Abfallspezifikation und Mengengerüst. *Report 278 /* (*GRS Köln*, 2011); https://www.grs.de/sites/default/files/pdf/GRS-278_neu.pdf.
43. Y. A. Akovali, Nuclear data sheets for A = 242. *Nuclear Data Sheets* **96**, 177–239 (2002).
44. P. Benetti, A. Cesana, A. Dodaro, S. Mongelli, G. L. Raselli, M. Terrani, F. Troiani, Production of ^{242m}Am. *Nucl. Instrum. Methods Phys. Res. A* **564**, 482–485 (2006).
45. M. Q. Buckner, C. Y. Wu, R. A. Henderson, B. Bucher, N. Wimer, A. Chyzh, T. A. Bredeweg, B. Baramsai, A. Couture, M. Jandel, S. Mosby, J. L. Ullmann, Comprehensive ^{242m}Am neutron-induced reaction cross sections and resonance parameters. *Phys. Rev. C* **95**, 061602 (2017).
46. A. Shimada, Y. Kameo, K. Takahashi, A new method to analyze ^{242m}Am in low-level radioactive waste based on extraction chromatography and β-ray spectrometry. *Anal. Chem.* **85**, 7726–7731 (2013).
47. M. Yamamoto, D. J. Assinder, J. Kuwabara, Curium isotopes and Americium-242m in Irish Sea sediment. *Radiochim. Acta* **83**, 121–126 (1998).
48. A. Sasahara, T. Matsumura, G. Nicolaou, D. Papaioannou, Neutron and gamma ray source evaluation of LWR high burn-up UO_2 and MOX spent fuels. *J. Nucl. Sci. Technol.* **41**, 448–456 (2012).
49. V. T. Bowen, H. D. Livingston, Americium-242m in nuclear test debris. *Nature* **256**, 482 (1975).

Acknowledgments: We thank P. Brozynski and S. Dubchak for assistance with sampling in Prypiat, M. Heller for assistance with measurements, and N. Evans for proofreading. **Funding:** This work was supported by the German Federal Ministry of Education and Research (contract numbers 02NUK044A and 02NUK044B) and Siebold Sasse Foundation. **Author contributions:** H.B. contributed to conceptualization, methodology, validation, formal analysis, investigation, writing, and visualization (original draft and editing). L.H. contributed to methodology, formal analysis, investigation, and writing (review and editing). M.W. contributed to methodology, investigation, and writing (review and editing). C.W. contributed to conceptualization, methodology, resources, writing, supervision, project administration, and funding acquisition. K.W. contributed to conceptualization, methodology, investigation, resources, writing, and administration. M.R. contributed to investigation, writing, and formal analysis (review and editing). N.K. contributed to methodology, investigations, and writing (review and editing). **Competing interests:** The authors declare that they have no competing interests. **Data availability statement:** All data needed to evaluate the conclusions in the paper are present in https://doi.org/10.25835/0008383.

Submitted 21 April 2021
Accepted 13 September 2021
Published 29 October 2021
10.1126/sciadv.abj1175

Citation: H. Bosco, L. Hamann, N. Kneip, M. Raiwa, M. Weiss, K. Wendt, C. Walther, New horizons in microparticle forensics: Actinide imaging and detection of ^{238}Pu and ^{242m}Am in hot particles. *Sci. Adv.* **7**, eabj1175 (2021).